Ann. Geophys. Discuss., https://doi.org/10.5194/angeo-2018-3
Manuscript under review for journal Ann. Geophys.
Discussion started: 11 January 2018

Annales Geophysicae Discussions Open Access

An investigation of the ionospheric F - region near the EIA crest in India using OI 777.4 and 630.0 nm nightglow observations

Authors:

1. **Navin Parihar**
   Equatorial Geophysical Research Laboratory,
   Indian Institute of Geomagnetism, Tirunelveli 627 011, India
   e-mail: navindeparihar@gmail.com

2. **Sandro M. Radicella**
   The Abdus Salam International Centre for Theoretical Physics,
   Strada Costiera 11, 34151 Trieste, Italy
   e-mail: rsandro@ictp.it

3. **Bruno Nava**
   The Abdus Salam International Centre for Theoretical Physics,
   Strada Costiera 11, 34151 Trieste, Italy
   e-mail: bnava@ictp.it

4. **Yenca Olivia Migoya Orue**
   The Abdus Salam International Centre for Theoretical Physics,
   Strada Costiera 11, 34151 Trieste, Italy
   e-mail: yenca@ictp.it

5. **Prabhakar Tiwari**
   Dr. K. S. Krishnan Geomagnetic Research Laboratory,
   Indian Institute of Geomagnetism, Allahabad 221 505, India
   e-mail: ptiwari@iigs.iigm.res.in

6. **Rajesh Singh**
   Dr. K. S. Krishnan Geomagnetic Research Laboratory,
   Indian Institute of Geomagnetism, Allahabad 221 505, India
   e-mail: rajeshsing03@gmail.com

Ann. Geophys. Discuss., https://doi.org/10.5194/angeo-2018-3
Manuscript under review for journal Ann. Geophys.
Discussion started: 11 January 2018

Corresponding Author:
Navin Parihar, Equatorial Geophysical Research Laboratory, Indian Institute of Geomagnetism, Krishnapuram, PO Maharaja Nagar, Tirunelveli - 627 011, India.
e-mail: navindeparihar@gmail.com

Ann. Geophys. Discuss., https://doi.org/10.5194/angeo-2018-3
Manuscript under review for journal Ann. Geophys.
Discussion started: 11 January 2018

Annales Geophysicae Discussions

Abstract

Simultaneous observations of OI 777.4 nm and OI 630.0 nm nightglow emissions were carried at a low latitude station, Allahabad (25.5º N, 81.9º E, geomag. lat. ~ 16.30º N), located near the crest of Appleton anomaly in India during September - December 2009. This study attempts to examine the behaviour of the F region of ionosphere using airglow derived parameters. Using an empirical approach put forward by Makela et al. (2001), firstly, we propose a novel technique to calibrate OI 777.4 and 630.0 nm emission intensities using *Constellation Observing System for Meteorology, Ionosphere, and Climate/Formosa Satellite Mission 3 (COSMIC/FORMOSAT-3)* electron density profiles. Next, electron density maximum (N_m) and its height (hmF2) of the F - layer have been derived from the information of two calibrated intensities. Nightglow derived Nm and hmF2 were in reasonable agreement with few measurements reported earlier. Nm and hmF2 were used to study the behaviour of the F - region over Allahabad on the limited number of nights. Nocturnal variation of Nm showed the signatures of the retreat of equatorial ionization anomaly (EIA) and mid-night temperature maximum (MTM) phenomenon that are usually observed in the equatorial and low-latitude ionosphere. Signatures of gravity waves having period in the range of 0.7 – 3.0 h were also seen in Nm and hmF2 variations. Sample Nm and hmF2 maps have also been generated to show the usefulness of this technique in studying the ionospheric processes.

1. Introduction

Ground-based airglow observations have been successfully used to derive physical parameters of the emitting region. Firstly, emission intensities are monitored using ground-based photometers or imaging systems, and then different parameters are derived from their intensity information. Examples are: atomic oxygen density (Lednyts'kyy et al., 2014; Russell et al., 2005), vertical transport (Broadfoot and Gardner, 2001; Hays et al., 2003), mesospheric temperatures (Innis et al., 2001; Scheer and Reisin, 2007; Holmen et al., 2014; Parihar et al., 2017, and references cited therein), mesospheric winds (Lloyd et al., 1990), density and pressure (Takahashi et al., 2004), thermospheric temperatures and wind velocities (Cocks, 1983; Vila et al., 1998; Ford et al., 2006, 2008; Nakamura et al., 2017), F region peak electron density and its height (Sahai et al., 1981; Makela et al., 2001), F region zonal drifts (Yao and Makela, 2007), etc.. Often the derived parameters are then utilized to understand the behaviour of the emitting region mainly its chemistry, dynamics and electrodynamics (Semenov, 1988; Fagundes et al., 2001; Makela et al, 2001; Shiokawa et al., 2003; Makela et al., 2004; Scheer and Reisin, 2007; Ford et al., 2008; López-González et al., 2009; Parihar et al., 2013; Holmen et al., 2014) Other ground-based techniques include lidars and radars; however, airglow experiments remain to be a favourite due to their well-established simplicity, cost-effectiveness and capability for continuous operation on longer timescale (Ford et al., 2008; Espy et al., 2011; Holmen et al., 2014; Scheer and Reisin, 2007). An important limitation with airglow measurements is that studies are limited to night-time and greatly depend on sky observing conditions.

Simultaneous measurement of OI 777.4 and 630.0 nm nightglow emissions has been successfully used to derive the F region peak electron density and its height; however, is limited to report by Sahai et al. (1981) and Makela et al. (2001). Theoretical foundation for deriving the electron density and corresponding peak using simultaneous measurements of two airglow emissions from the F - region was laid by Tinsley and Bittencourt (1975). Using correlative study of airglow measurements with the ionosonde measured parameters, Sahai et al. (1981) noted good correlation between (i) $\sqrt{I_{7774}}$ and Nm, and (ii) $(\sqrt{I_{7774}})/I_{6300}$ and hmF2 where I_{7774} and I_{6300} are OI 777.4 and 630.0 nm emission intensities, respectively; while, Nm and hmF2 are the F region peak electron density and its height, respectively. Subsequent improvement in this technique was done by Makela et al. (2001). These authors generated spatial (topographic) maps of the F region of ionosphere using all-sky observations of these two emission features. A topographic map of ionosphere features the 3-D representation of electron density and height of the F - region of the ionosphere.

In this study, using formulations outlined by Makela et al. (2001), firstly, OI 777.4 and 630.0 nm emission intensities have been empirically calibrated to Rayleigh units with the help of *Constellation Observing System for Meteorology, Ionosphere, and Climate/Formosa Satellite Mission 3 (COSMIC/FORMOSAT-3)* electron density profiles; and then, Nm and hmF2 have been derived from two calibrated intensities at Allahabad (25.5º N, 81.9º E), India during September - December 2009. An overview of the underlying principle behind these measurements of ionospheric parameters has been also presented. Next, limited data of derived Nm and hmF2 have been used to study the nocturnal behaviour of the F region over Allahabad. Sample Nm and hmF2 maps have been also generated to illustrate the usefulness of this technique in understanding the ionospheric processes like equatorial plasma bubbles.

2. Underlying theory

The basis of determining Nm and hmF2 lays in the excitation mechanisms of OI 777.4 and 630.0 nm emissions (Sahai et al., 1981; Makela et al., 2001). During nighttime, the following recombination reaction involving the O^+ ion and electron is the principal source of OI 777.4 nm emission (Tinsley et al., 1973):

$$\mathbf{O^+} \quad + \quad \boldsymbol{e} \quad \rightarrow \quad \mathbf{O}\,(^5\mathrm{P}) \tag{1}$$

Ignoring the contribution of the ion-ion recombination mechanism to OI 777.4 nm emission (Tinsley et al., 1973), its intensity (I_{7774}) depends upon the product of O^+ ion concentration, $[O^+]$, and electron density, n_e. Assuming the quasi-neutral ionospheric plasma to be mainly composed of O^+ ions and electrons, its intensity can be seen depends on $n_e(h)^2$ where $n_e(h)$ is the electron density at height h. Now $n_e(h)$ is related with Nm through well-known Chapman's function (Tinsley et al., 1973). After detailed numerical computation and correlative study involving Mass Spectrometer Incoherent Scatter (MSIS-86) model (Hedin, 1987) and International Reference Ionosphere 1995 (IRI-95) model (Bilitza, 1997), Makela et al. (2001) arrived to the following empirical equation:

$$N_m = [3.06 \times \sqrt{I_{7774}} - 1.11] \times 10^{11} \tag{2}$$

where Nm is in m^{-3}. Subsequently, the critical frequency of the F2 - layer, foF2, in MHz, can be estimated using the following expression (Tinsley et al., 1973):

$$N_m = 1.24 \times 10^4 \times (foF2)^2 \tag{3}$$

Ann. Geophys. Discuss., https://doi.org/10.5194/angeo-2018-3
Manuscript under review for journal Ann. Geophys.
Discussion started: 11 January 2018

Next, the determination of hmF2 is based on the chemistry of OI 630.0 nm emission. During nighttime, this emission feature is primarily due to the following dissociative recombination reaction involving O_2^+ ion and electron (Link and Cogger, 1988):

$$\mathbf{O_2^+} + \boldsymbol{e} \rightarrow \mathbf{O}^* (^1D) + \mathbf{O} \quad (4)$$

However, the formation of O_2^+ ion is due to charge exchange between molecular oxygen, O_2, and O^+ ion as

$$\mathbf{O^+} + \mathbf{O_2} \rightarrow \mathbf{O_2^+} + \mathbf{O} \quad (5)$$

Thus, the production of O_2^+ strongly depends upon both the O_2 density and the height of the F - layer. Because of this $[O_2]$ association, the intensity of OI 630.0 nm (I_{6300}) depends upon the height of the F – layer apart from the electron density. Link and Cogger (1988) found that the intensity of this emission depends on $[N_2]$ and $[O_2]$ of the neutral atmosphere. As the density of neutral atmosphere decreases exponentially with height around the OI 630.0 nm emission altitude, such dependency is also likely to exist between its intensity and the height of F - layer. Using the emission rate of OI 630.0 nm nightglow given by Link and Cogger (1988), and adopting the approach of Tinsley and Bittencourt (1975) and Sahai et al. (1981), Makela et al. (2001) arrived at the following expression relating the $\sqrt{(I_{7774})} / I_{6300}$ ratio with the height of the F – layer:

$$hmF2 = e^{0.171 \times ln[\sqrt{I_{7774}} / I_{6300}] + 6.43} \quad (6)$$

This expression has been used to determine the height of the peak of electron density in the present study.

3. Experimental set up and data:

Simultaneous observations of OI 777.4 and 630.0 nm nightglow emissions were carried out at a low latitude station Allahabad (25.5º N, 81.9º E, geomagnetic lat. ~ 16.5º N), India, located near the crest of ionization anomaly, during September - December 2009. An all-sky imager (Keo Scientific Ltd., Canada made) was operated to monitor the nightglow emissions under clear sky conditions and around new moon period. This imaging system is described in detail by Parihar and Taori (2015). The interference filters having bandwidth of ~ 2 nm and transparency in the 66 – 77 % range were utilized to monitor the OI 777.4 nm, 630.0 nm and background emission at 530 nm with the exposure time of 90 s. The signal-to-noise ratio for these settings of imaging was better than 22.6 decibels. The observations of OI 557.7 nm and OH broadband emissions were also made. The time duration of each sequential observation was 9 minutes. On each night, a flat-field image was taken during the start of imaging

Ann. Geophys. Discuss., https://doi.org/10.5194/angeo-2018-3
Manuscript under review for journal Ann. Geophys.
Discussion started: 11 January 2018

observations, and subsequent images recorded by the imaging system were divided by this flat-field image to approximately account for artefacts due to van Rhijn effect and pixel-to-pixel non-uniformity of the CCD detector. Using known astral positions, the location of zenith was identified in airglow images. For simplicity, average intensity of a square bin [corresponding to a field of view of ~ 1° along zenith at an altitude of 250 km] in imaging observations has been considered. Such consideration will help in comparing results of the electron density and height measurements with those of ionosonde and FORMOSAT-3/COSMIC observations. Using this intensity and timestamp information of each image, intensity time series was generated and used in this study. The details of this technique is discussed elsewhere (Parihar and Taori, 2015; Parihar et al., 2017).

Assuming that the transmission of filters and sensitivity of CCD detector are the main source of experimental error, the uncertainty in the intensity measurements is estimated to be ~ 8 %. Using this information, the errors in airglow derived Nm, hmF2 and foF2 has been estimated and the derived quantities are uncertain by 1.68 x 10^{10} m^{-3}, 5.56 km and 0.14 MHz, respectively. Nightglow observations were severely affected by the presence of clouds during September; while, the foggy weather conditions affected observations during November - December. Consequently, good quality data of 14 nights only were available for a meaningful study. Mostly, the duration of continuous observation on each night was typically 6 – 8 hours, and the Nm/foF2/ hmF2 dataset consisted of ~ 40 – 60 measurements. On these nights, geomagnetic activity index, Ap, lay between 0 and 13 units and F10.7 cm solar flux varied in the range of 69 – 82 units (http://isgi.latmos.ipsl.fr, www.swpc.noaa.gov). Majority of the nights (about 9) fell in the category of quiet nights with 14 October being the quietest one. Most geomagnetically disturbed one was 22 October.

COSMIC/FORMOSAT-3 data: COSMIC/FORMOSAT-3 is a joint Taiwan-US mission that utilizes Radio Occultation (RO) technique to determine physical parameters like temperature, pressure, water vapour, electron density, total electron content, scintillation S4 index etc. (Anthes et al., 2008). The COSMIC electron density data were downloaded from the COSMIC Data Analysis and Archive Center (CDAAC, http://cdaac-www.cosmic.ucar.edu/cdaac/index.html).

Ionosonde data: A state-of-art Canadian Advanced Digital Ionosonde (CADI) system is permanently installed at Allahabad and carries out the vertical soundings in 1 – 20 MHz frequency range. Due to some technical issues associated with CADI, few hours of ionosonde data was available on 16 September 2009.

4. Calibration of OI 777.4 and 630.0 nm intensities:

Nm and hmF2 derivation using the empirical expressions (2) and (6) utilize calibrated emission intensities in Rayleigh. In our case, absolute calibration of emission intensities was not possible due to lack of standard low brightness source. Under similar situation, Makela et al. (2001) utilized the collocated radar measurements of the electron density and height to calibrate OI 777.4 nm and 630.0 nm intensities in their investigations using expressions (2) and (6). *Calibration term* is a factor that converts the observed intensity of an emission feature from arbitrary units to Rayleighs. Similarly herein, the coincidental COSMIC electron density profiles in the latitude-longitude grid of 5º x 5º centred on Allahabad have been used to calibrate the two intensities. Such approach is based on the comparison of the electron density profiles derived from COSMIC RO measurements and ground-based ionosonde measurements reported lately by Hu et al. (2014) and Limberger et al. (2015). Hu et al. (2014) compared the COSMIC Nm values with the ionosonde measurements at four stations over China spread in the 18 – 54º N latitude range and noted correlation of 0.90 or more amongst the two measurements. Limberger et al. (2015) studied the Nm/hmF2 measurements inferred from the COSMIC/FORMOSAT-3 electron density profiles and performed its global comparison with the ionosonde measurements 2006-2014. These authors found a correlation coefficient of 0.94 and 0.76 between the COSMIC and ionosonde measurements for Nm and Hm, respectively, in the geomagnetic latitude range of 0 – 20º. Coinciding with our experiments, two COSMIC coincidences were available in the 5º x 5º latitude-longitude grid over Allahabad – one each on 14 October and 11 December 2009 (hereafter CP1 and CP2, respetively). These COSMIC electron density profiles were checked for data quality and are shown in Figure 1. The azimuthal smearing of the tangent point trajectory COSMIC profiles CP1 and CP2 are also tabulated in Table 1. Using Nm and hmF2 information of each COSMIC profile, corresponding OI 777.4 nm and OI 630.0 nm intensity was estimated using equation (3) and (7), respectively. Using this estimated intensity and observed one; the calibration term for both emissions was derived. Table 1 summarizes the calibration factors obtained using two COSMIC profiles. Figure 2 presents a typical example of nocturnal variation of two calibrated intensities on 24 October 2009 using CP1 calibration terms. Table 1 clearly indicate dissimilar values of calibration terms inferred from CP1 and CP2 for each emission, thereby making it difficult to infer suitable calibration factor. Next, a comparison of airglow derived quantities with coincidental ionosonde measurements on 16 September 2009 was performed to identify the suitable *calibration term*.

On the first, two datasets of calibrated intensities corresponding to each set of calibration factors were generated. Next, the critical frequency of F2-layer (foF2) and the peak height of electron density (hmF2) were derived using equations (2), (3) and (7) from each dataset. For convenience, *Case I (CP1)* refers to the foF2 - hmF2 dataset derived from the two emission intensities calibrated using CP1, and Similarly, *Case II (CP2)* addresses the ionospheric measurements when second calibration set inferred from CP2 is used for calibrating intensities. Table 2 summarizes the two sets of the airglow derived quantities along with the ionosonde measurements. The closest coincidences in time have been considered for better comparison. It is clear from Table 2 that *Case I (CP1)* dataset appears to be more realistic and is in better agreement with the ionosonde measurements in comparison to *Case II (CP2)* dataset. In *Case I (CP1)*, hmF2 (height of electron density peak), and hpF2 (virtual height at 0.834 foF2) vary by 10 km or less. Batista et al. (1991) have reported such departures in hmF2 and hpF2 during nighttime. On the other hand, the difference between hmF2 and hpF2 is fairly large in *Case II (CP2)*. Hence, two intensities calibrated using *CP1 calibration terms* have been used to derive Nm and hmF2 for studying the behaviour of the F region over Allahabad. Nm and hmF2 derived from two intensities using *CP2 calibration terms* have also been discussed. Herein, the calibration of intensities strongly depends upon the experimental set up, exposure times and CCD characteristics which were kept unchanged during September - December 2009. Hence, *calibration term* is assumed to hold good for entire data.

5. Observations, results and discussions:

5.1 Nm and hmF2 measurements:

Figure 3 and Figure 4 present the frequency of occurrence of derived Nm and hmF2, respectively during September – December 2009. In both figures, black bars represent the F region measurements using CP1 calibration term; while, those in red depict measurements using CP2 calibration term. Hereafter, Nm derived using CP1 and CP2 calibrated intensities are termed as Nm^{CP1} and Nm^{CP2}; while, hmF2 derived using CP1 and CP2 calibration are referred to as $hmF2^{CP1}$ and $hmF2^{CP2}$. Nm^{CP1} measurements are in the range of 0.9 – 3.2 x 10^{11} m^{-3}; while, Nm^{CP2} values were ~ 0.7 – 1.0 x 10^{11} m^{-3} lesser than corresponding Nm^{CP1} measurements. Nm^{CP1} was seen to vary in the range of 1.2 – 2.1 x 10^{11} m^{-3} in about 59 % of measurements. Nm^{CP2} measurements usually lay in the range of 0.3 – 1.4 x 10^{11} m^{-3}. During

Ann. Geophys. Discuss., https://doi.org/10.5194/angeo-2018-3
Manuscript under review for journal Ann. Geophys.
Discussion started: 11 January 2018

EIA and MTM events, Nm values were relatively higher, and will be discussed later. Prominent peak in occurrence of Nm^{CP1} and Nm^{CP2} centred about 1.7 x 10^{11} m^{-3} and 1.0 x 10^{11} m^{-3}, respectively, can clearly be seen in Figure 3. Unlike Nm measurements, derived hmF2 was found to vary in two ranges, and $hmF2^{CP1}$ values were usually 40 – 60 km lesser than corresponding $hmF2^{CP2}$ measurements. These facts can clearly be seen in Figure 4. $hmF2^{CP1}$ was found to vary between 230 and 260 km in about 60 % of cases; while, $hmF2^{CP2}$ was observed in lay in the range of 278 – 304 km in about 43 % of measurements. This lower hmF2 spectrum was centred on around 246 and 294 km for CP1 and CP2 calibration. However, second range of the F region peak heights were near uniformly spread over 254 – 276 km for $hmF2^{CP1}$ measurements and over 306 – 332 km for $hmF2^{CP2}$ measurements. Overall, mean Nm^{CP1} and Nm^{CP2} is 1.69 ± 0.18 x 10^{11} m^{-3} and 0.99 ± 0.14 x 10^{11} m^{-3}, respectively; while, mean $hmF2^{CP1}$ $hmF2^{CP2}$ is 258.4 ± 8.2 km and 309.3 ± 9.8 km, respectively. Further, foF2 were estimated from airglow derived Nm^{CP1} and Nm^{CP2} using equation (3) (hereafter, referred to as $foF2^{CP1}$ and $foF2^{CP2}$, respectively). The $foF2^{CP1}$ measurements were found to swing between 2.1 and 5.1 MHz; while, $foF2^{CP2}$ lay in the range of 1.2 – 4.2 MHz.

Comparison with earlier reports: Using digital ionosonde measurements at a nearby station Bhopal (23.2° N, 77.6° E, geomag. lat. ~ 14.4° N), Yadav et al. (2010) studied the diurnal and seasonal variation of foF2 and hmF2 during the solar minimum period of 2007. During pre-midnight hours, they found the median values of foF2 were between ~ 2.9 and 5.4 MHz during September-October equinox; while, we observed $foF2^{CP1}$ and $foF2^{CP2}$ in the range of 3.0 – 4.4 and 2.1 – 3.5 MHz, respectively. During the post-midnight hours, Yadav et al. (2010) observed foF2 in 2.2 – 3.0 MHz range; whereas, derived $foF2^{CP1}$ and $foF2^{CP2}$ were in the range of 3.3 – 4.0 and 2.4 – 3.1 MHz, respectively. During the passage of the crest of EIA and MTM over Allahabad, comparatively higher values were noted as high as ~ 5.2 and 4.2 Mhz for $foF2^{CP1}$ and $foF2^{CP2}$ measurements, respectively. Luan et al. (2015) have studied the behaviour of the EIA using Nm and hmF2 retrieved from COSMIC database during 2007 - 2012. At 2000 LT during solstice of December 2008, their NmF2 maps suggest Nm values in the range of 2 – 4 x 10^{11} m^{-3} near Allahabad. In our measurements, Nm^{CP1} and Nm^{CP2} values are found to vary in the range of 1.6 – 2.0 x 10^{11} m^{-3} and 0.9 – 1.3 x 10^{11} m^{-3}, respectively, during 1930 – 2030 h. Further, Yadav et al. (2010) found hmF2 to vary in the 240 – 302 km range; whereas, derived $hmF2^{CP1}$ $hmF2^{CP2}$ vary in the range of 230 – 280 km and 280 – 330 km, respectively. Using digital ionosonde measurements, Sethi et al. (2004) studied the

Ann. Geophys. Discuss., https://doi.org/10.5194/angeo-2018-3
Manuscript under review for journal Ann. Geophys.
Discussion started: 11 January 2018

behaviour of hmF2 over New Delhi (27º N), India during 2001 – 2002 (a period of high solar activity). During the night, they found the median value of hmF2 to vary between 290 and 350 km in the equinoctial months.

5.2 Nocturnal behaviour of Nm: Signatures of EIA and MTM

Typical examples of the airglow derived Nm and hmF2 of the F – layer over Allahabad during October and December 2009 are shown in Figure 5 (a) – (d). Nm and hmF2 are presented in the top and bottom panel, respectively. For simplicity, Nm and hmF2 derived from two intensities using *CP1 calibration terms* have been presented and discussed herein. Figure 6 present the variation of Nm and hmF2 on 14 October, 22 October (a slightly geomagnetically disturbed day), and 20 November. Nocturnal variation of the Nm displayed the common behaviour noted globally at low latitudes (Danilov and Vanina-Dart, 2010; Chakraborty and Hajra, 2009, and references cited therein). On most nights (especially in October), the Nm variations during pre-midnight hours were marked by the signatures the retreat of equatorial ionization anomaly (EIA) as an elevated peak during 2100 – 2400 h (mostly during October). As for example, the EIA peak was noted during 2100 – 2300 h on 14, 21 and 24 October 2009. On slightly disturbed night of 22 October and 20 November, the EIA peak was noted during 2230 – 2400 h (about 1 – 2 h later in comparison to its occurrence on the quiet nights, see Figure 6). During the maximum of EIA on 21 and 24 October, Nm was found to reach ~ 3.2×10^{11} m^{-3}. At Allahabad with the geomagnetic latitude of ~ 16.5º N, the presence of such peaks corresponding to EIA is not unusual. EIA is well known feature of low-latitude ionosphere. The crests in ionization are formed on both sides of the geomagnetic equator by the combined effects of the upward E x B plasma drift and the ambipolar diffusion along geomagnetic field lines during morning-noon hours, progress towards off-equatorial geomagnetic latitudes of about ± 18°, and retreat back towards equator during nighttime. EIA development strongly depends on (i) the strength of eastward electric field; and (ii) the transport of ionospheric plasma along the field lines (controlled by the rate of diffusion and neutral winds) (Rastogi and Klobuchar, 1990; Pavlov, 2006; Chakraborty and Hajra, 2009; and references cited therein). Hence, one possible explanation is that strong upward E x B drift occurred at geomagnetic equator that lifted the ionization to higher altitudes which then diffused to off-equatorial latitudes beyond that of Allahabad. Moreover these observations of the EIA crests are in the winter months of October – December; the transequatorial neutral winds blowing across the summer-winter hemisphere might have possibly pushed the EIA to latitudes as high as Allahabad (Luan et al., 2015). Our results on the observations of EIA are in reasonable agreement with some of earlier reports (Rao and Malhotra, 1964; Rama Rao et al., 1977; Lin et al., 2007; Chakraborty and Hajra, 2009; Zhao et al., 2009). Studies by Rao and Malhotra (1964) on the latitudinal variation of foF2 in Asian sector suggest that EIA can persist at least until 0200 LT at ~ 30º dip latitude. Using 40 MHz radio beacon signals, Rama Rao et al. (1977) investigated diurnal variation of TEC over Waltair (18º N), India and found well-defined decrease of anomaly during 1900 – 2145 h LT during the equinox months. Study of time evolution of EIA by Lin et al. (2007) using FORMOSAT-3/COSMIC data of July - August 2006 suggests the presence of decayed EIA during 1900 – 2300 LT around 15° geomagnetic latitude with Nm in 2 – 5 x 10^{11} m^{-3} range. Using GPS-TEC measurements, Chakraborty and Hajra (2009) and Zhao et al. (2009) have investigated the EIA characteristics over Calcutta (23º N), India during 1978-1990 and in the Asian-Australian sector (50º N – 30º S, 95º E – 135º E) during 1996-2004, respectively. Apart from usual daytime TEC maximum, Chakraborty and Hajra (2009) noted a secondary maximum in TEC variations during 1800 – 2000 h IST which were highly correlated with the equatorial electrojet (EEJ) strength. Zhao et al. (2009) observed (i) the EIA crest to appear during 2000 - 2200 h LT near 20 – 22º N latitude during December - February, and (ii) the behaviour of EIA to be more dependent of solar activity near the regions of anomaly crest. Using chain of seven ionosonde station spread in 10 – 29° N latitude range in India, Yadav et al. (2013) investigated the latitudinal shifting of EIA crest, and found EIA crest during equinoxes to appear at around 21º, 24º and 26º N, respectively, for low, moderate, and maximum solar activity of the 19th solar cycle.

Around midnight, Nm was observed to reach its minimum during 0000 – 0200 h on most occasions. Beyond 0200 h, an additional shallow hump in Nm variations was observed around 0300 h. Such behaviour can clearly be seen on 21 October and 14 December (shown in Figure 5). Such a feature in the thermospheric nightglow measurements has been linked to the midnight pressure bulge/temperature maximum phenomena (MTM) (Rao and Sastri, 1994; Batista et al., 1997; Mukherjee et al., 2006; Shepherd, 2016; Figueiredo et al., 2017). MTM refers to an unusual large-scale increase in the thermospheric temperatures in the equatorial region around mid-night hours due to convergence of (i) eastward zonal wind driven by the day-to-night differential heating, (ii) upward propagating tides and (iii) in-situ thermospheric tides produced by EUV associated heating. This convergence reverses the flow of the thermospheric meridional wind from equatorwards towards the poles; thereby, pushing plasma to off-equatorial latitudes. This causes an increase in recombination reaction; hence, an enhancement of OI 777.4 and 630 nm emission intensity (Figueiredo et al., 2017, and references cited therein). On 20 November, a sharp ascend of Nm (shown in Figure 6) as a consequence of MTM phenomena is observed; however, its descent appears to be possibly masked by the dawn time enhancement of electron density. During such events, MTM associated peak was usually observed around 0300 h IST (as can be seen in Figure 5 and 6). Studies using Doppler width measurements of OI 630.0 nm nightglow over an equatorial station Kavalur (12.5° N), India during 1992-1993 by Rao and Sastri (1994) indicate MTM to occur usually an hour after midnight during winter. Mukherjee et al. (2006) studied the behaviour of OI 630.0 nm nightglow at a low latitude station Kolhapur (17° N), India during December 2002 – April 2003 and found the MTM associated peaks to occur mostly during 0200 – 0300 LT. Overall, the behaviour of Nm during the night was characterized by (i) the signatures of ionization anomaly in pre-midnight sector, (ii) a minimum around 0000 – 0200 h, and (iii) a hump as a consequence of midnight temperature maximum phenomena beyond 0200 h. Sometimes a monotonous decrease of Nm throughout the night was also noted (e. g. on 22 October in Figure 6).

5.3 Nocturnal behaviour of hmF2

As pointed out earlier, hmF2 was usually observed to vary in two ranges during the night: sometimes between around 230 and 260 km, and else in the range of ~ 250 - 285 km. As for example, hmF2 variations were found to lay in the 230 - 250 km range on 20 November (shown in Figure 6). As can be seen in Figure 5 and 6, hmF2 was generally found to increase during the pre-midnight hours. For example, hmF2 went up from ~ 260 km to ~ 279 km on 15 October. On 21 October, comparatively sharp change in hmF2 (from 230 to 270 km) is seen during 2130 – 2330 h. On this night, the nocturnal variation of 777.4 nm intensity was characterized by a peak corresponding to the motion of EIA during 2130 – 2300 h. However, its signature was not seen in 630.0 nm intensity variation that rather showed a decrease. As OI 630.0 nm emission intensity depends on both the electron density and height of the F layer, an increase in the height of F-layer is interpreted. hmF2 found to increase from 236 to 256 km during 2130 – 2300 h. Similar situation was observed on 24 October (shown in Figure 2) during 2130 – 2300 h; however, the height change was less (from 246 to 255 km) in comparison to that observed on 21 October. In the post-midnight sector, hmF2 was found to attain its maximum during 0000 – 0200 h and then decrease during rest of the night. During the occurrence of MTM, the lowering of hmF2 in ~ 10 – 20 km range was observed. This can clearly be seen on 21 October, 20 November and 14 December in Figure 5 and 6. To compare, Mukherjee et al. (2006) observed large height decent of the F - layer in ~ 20 – 60 km range. Overall, hmF2 was found to increase in the pre-midnight hours, attain a maximum around 0000 – 0200 h and then decrease beyond 0200 h. Nearly similar behaviour of hmF2 has been reported by Sethi et al. (2004). During the night, Sethi et al. (2004) found the minimum of hmF2 at ~ 1900 LT, an increase thereafter followed by few shallow peaks around mid-night and in the post-midnight hours. Atypical hmF2 variations were also observed. For example, (i) wave-like features on 22 October, and (ii) a gradual increase in hmF2 from 245 to 264 km throughout the night on 24 October, and (iii) comparatively the large variations in hmF2 (in the 250 – 300 km range) on slightly disturbed night in comparison with those observed on quiet and moderate nights (see Figure 6). Matching with our observations on 24 October, Sethi et al. (2004) observed an increase in hmF2 till pre-sunrise hours at ~ 0500 LT sometimes especially during winter and equinox months.

5.4 Signatures of gravity waves in Nm and hmF2 variations

Nocturnal variations of Nm and hmF2 were often marked by short-period (~ 1 – 3 h) wave-like features. As for example, (i) Nm variations on 15 October were marked by about 1.3 h period wave-like oscillation during 2230 – 0100 h; however, this wave was not seen hmF2 variations, (ii) a 0.8 h period wave was noted in Nm variations during 0000 – 0200 h on 22 October; while, hmF2 variations showed the presence of wave-like oscillation of period ~ 2.4 h, (iii) 1.5 – 2.0 h waves were noted in Nm and hmF2 variations on 23 October. Sometimes similar waves were noted in both Nm and hmF2 variation. For example, a ~ 0.9 h period wave was seen in both Nm and hmF2 variations on 14 December. Overall, short period (0.7 – 3 h) wavelike oscillations were noted in Nm and hmF2 variations. While estimating the wave-periodicities, Nm and hmF2 variations during the presence of EIA and MTM have been excluded. Several investigators have reported the presence of such wavelike features in the ionospheric parameters. Using CADI measurements, Klausner et al. (2009) studied the seasonal variation of gravity wave in virtual height of the F2 layer at Sao Jose dos Campos (23.2° S, 45.9° W), a low latitude station located under the southern crest of EIA in Brazil and noted the presence of 30 – 180 min waves. Ford et al. (2006, 2008) investigated the thermospheric gravity wave activity in temperature and wind velocities inferred from Fabry-Perot Interferometers based measurements of OI 630.0 nm emission over northern Scandinavia during 2000 – 2006, and found the presence of waves with period ranging from few tens of minutes to eight hours. Using all-sky imaging observations of OI 630.0 nm

Ann. Geophys. Discuss., https://doi.org/10.5194/angeo-2018-3
Manuscript under review for journal Ann. Geophys.
Discussion started: 11 January 2018

emission, Paulino et al. (2016) studied the presence of thermospheric gravity waves over São João do Cariri (7.4° S), Brazil during 2000 – 2010. Most of the observed waves had period between 5 and 45 min in their study.

5.5 Nm and hmF2 maps over Allahabad:

Success of airglow derived Nm and hmF2 in investigating the behaviour of EIA, MTM and gravity waves motivated us to extend this study to imaging observations. On one occasion (on 09 January 2016), coincidental ionosonde and COSMIC measurements were available along with airglow experiments. Similar calibration approach was adopted using COSMIC data and Nm and hmF2 were derived from the calibrated intensity. Next, a limited comparison of airglow derived Nm and hmF2 with ionosonde measurements was done. Figure 7 presents the results of such comparison for Nm measurements. Airglow and ionosonde measurements are denoted by blue asterisks (*) with error bars and solid red circles (●), respectively. A reasonable agreement between airglow derived Nm and ionosonde measurements can be seen. However, disparity between two measurements for hmF2 was noted. Further, we extended this technique to generate Nm and hmF2 maps over 23 – 28° N x 82 – 85° E geographic grid on this night. Figure 8 and 9, respectively, presents sequence of Nm and hmF2 maps during 2000 – 2200 h. In Nm maps, the signatures of plasma depletions and their drift can clearly be seen. Most depleted regions had electron density of ~ 0.3 x 10^{11} m^{-3} or less. However, a decrease in the height of the F layer from 290 to 260 km till 2100 h, and an increase afterwards to 290 km can be noted in the hmF2 maps.

6. Discussions and future work:

In the present study, Nm and hmF2 have been estimated from OI 777.4 and 630.0 nm emission intensities using the empirical equations derived by Makela et al. (2001). Due to the lack of standard low brightness calibration source, intensities were not in Rayleigh units. An indirect approach was adopted to calibrate them using COSMIC electron density profiles. Coinciding with our experimental epoch, two such profiles were available that resulted in despairingly different sets of *calibration terms*. Consequently, two sets of derived Nm and hmF2 were generated. Two Nm measurements were different by ~ 0.7 x 10^{11} m^{-3}; while, a difference of ~ 50 km was seen in two hmF2 measurements. Clearly, strong dependence of derived Nm on the *calibration terms* used can be seen and this influences the accuracy of measurements. Present study being restricted to 14 nights of data, limits us to infer suitable set of *calibration terms*. An extensive coincidental database of airglow, ionosonde and

COSMIC measurements shall be taken up in future to validate the trustworthiness of this empirical calibration technique, and to achieve more accuracy in derived Nm and hmF2.

7. Conclusions:

This study is an attempt to investigate the behaviour of the F region from airglow perspective. Simultaneous measurements of OI 777.4 and 630.0 nm nightglow emissions were carried out at Allahabad (26° N), India during September - December 2009. Using the empirical approach of Makela et al. (2001), two airglow intensities were calibrated to Rayleigh units with the help of COSMIC electron density profiles. Next, the characteristics of the F region viz. Nm and hmF2 have been derived using airglow measurements. Initial results obtained herein appear to be promising with regards to Nm and hmF2 measurements when airglow intensities are accurately calibrated using COSMIC electron density profiles. Nocturnal variations of Nm and hmF2 were used to study the behaviour of the F region on limited number of nights. Signatures of the retreat of EIA and MTM, commonly observed in the equatorial and low latitude ionosphere, were noted in Nm variations. Nocturnal behaviour of hmF2 was similar to that reported earlier by Sethi et al. (2004). Wavelike oscillations having periodicities in the range of 0.7 – 3.0 h were seen in Nm/hmF2 variations. Severe limitation of this study is limited airglow data. We plan to extend this study to a larger database so as to achieve more accuracy in Nm and hmF2 measurements, and substantiate their use to understand the electrodynamics of the equatorial and low latitude ionosphere from airglow perspective.

Acknowledgements:

Funds for airglow research at Indian Institute of Geomagnetism are being provided by Department of Science and Technology (DST), Govt. of India, New Delhi. UCAR/COSMIC Program is gratefully acknowledged for providing COSMIC electron density profiles via http://cdaac-www.cosmic.ucar.edu/cdaac/index.html. Ionosonde data provided by S. Sripathi is gratefully acknowledged. Navin Parihar gratefully acknowledges the award of *Junior Associateship* by International Centre for Theoretical Physics, Trieste, Italy.

References:

Anthes, R. A., Ector, D., Hunt, D. C., Kuo, Y-H., Rocken, C., Schreiner, W. S., Sokolovskiy, S. V., Syndergaard, S., Wee, T-K., Zeng, Z., Bernhardt, P. A., Dymond, K. F., Chen, Y., Liu, H., Manning, K., Randel, W. J., Trenberth, K. E., Cucurull, L., Healy, S. B., Ho, S-P., McCormick, C., Meehan, T. K., Thompson, D. C., Yen, N. L.: The COSMIC/FORMOSAT-3 Mission: Early Results, Bull. Amer. Meteor. Soc., 89, 313–333, doi:10.1175/BAMS-89-3-313, 2008.

Batista, I. S., de Paula, E. R., Abdu, M. A., Trivedi, N. B.: Ionospheric effects of the March 13, 1989 magnetic storm at low and equatorial latitudes, J. Geophys. Res., 96, 13943-13952, 1991.

Batista, I. S., Sastri, J. H., deMedeiros, R. T. and Abdu, M. A.: Nighttime thermospheric meridional winds at Cachoeira Paulista (23°S, 45°W): Evidence for effects of the equatorial midnight pressure bulge, J. Geophys. Res., 102(A9), 20059-20062, doi:10.1029/97JA01387, 1997.

Broadfoot, A. L., Gardner, J. A.: Hyperspectral imaging of the night airglow layer from the shuttle: A study of temporal variability, J. Geophys. Res., 106, A11, 24795-24812, 2001.

Chakraborty, S. K. and Hajra, R.: Electrojet control of ambient ionization near the crest of the equatorial anomaly in the Indian zone, Ann. Geophys., 27, 93-105, doi:10.5194/angeo-27-93-2009, 2009.

Cocks, T. D.: Dual Fabry-Perot spectrometer measurements of daytime thermospheric temperature and wind velocity - Data analysis procedures, Applied Optics, 22, 726-732, doi:10.1364/AO.22.000726, 1983.

Danilov, A. D., Vanina-Dart, L. B.: Behavior of foF2 and hmF2 after sunset, Geomagnetism and Aeronomy, 50, 6, 796-803, doi:10.1134/S0016793210060113, 2010.

Espy, P. J., Ochoa Fernández, S., Forkman, P., Murtagh, D., and Stegman, J.: The role of the QBO in the inter-hemispheric coupling of summer mesospheric temperatures, Atmos. Chem. Phys., 11, 495-502, doi:10.5194/acp-11-495-2011, 2011.

Fagundes, P. R., Sahai, Y., Bittencourt, J. A.: Thermospheric zonal temperature gradients observed at low latitudes, Ann. Geophys., 19, 9, 1133-1139, doi:10.5194/angeo-19-1133-2001.

Figueiredo, C. A. O. B., Buriti, R. A., Paulino, I., Meriwether, J. W., Makela, J. J., Batista, I. S., Barros, D., and Medeiros, A. F.: Effects of the midnight temperature maximum observed in the thermosphere–ionosphere over the northeast of Brazil, Ann. Geophys., 35, 953-963, doi:10.5194/angeo-35-953-2017, 2017.

Ford, E. A. K., Aruliah, A. L., Griffin, E. M., and McWhirter, I.: Thermospheric gravity waves in Fabry-Perot Interferometer measurements of the 630.0 nm OI line, Ann. Geophys., 24, 555-566, doi:10.5194/angeo-24-555-2006, 2006.

Ford, E. A. K., Aruliah, A. L., Griffin, E. M., and McWhirter, I.: Statistical analysis of thermospheric gravity waves from Fabry-Perot Interferometer measurements of atomic oxygen, Ann. Geophys., 26, 29-45, doi:10.5194/angeo-26-29-2008, 2008.

Hays, P. B., Kafkalidis, J. F., Skinner, W. R., Roble, R. G.: A global view of the molecular oxygen night airglow, J. Geophys. Res., 108, D20, 4646, doi:10.1029/2003JD003400, 2003.

Holmen, S. E., Dyrland, M. E., Sigernes, F.: Long-term trends and the effect of solar cycle variations on mesospheric winter temperatures over Longyearbyen, Svalbard (78° N), J. Geophys. Res., 119, 6596-6608, doi:10.1002/2013JD021195, 2014.

Hu, L., Ning, B., Liu, L., Zhao, B., Li, G., Wu, B., Huang, Z., Hao, X., Chang, S., Wu, Z.: Validation of COSMIC ionospheric peak parameters by the measurements of an ionosonde chain in China, Ann. Geophys., 32, 1311-1319, 2014.

Innis, J. L., Phillips, F. A., Burns, G. B., Greet, P. A., French, W. J. R., and Dyson, P. L.: Mesospheric temperatures from observations of the hydroxyl (6–2) emission above Davis, Antarctica: A comparison of rotational and Doppler measurements, Ann. Geophys., 19, 359-365, doi:10.5194/angeo-19-359-2001, 2001.

Klausner, V., Fagundes, P. R., Sahai, Y., Wrasse, C. M., Pillat, V. G., and Becker-Guedes, F.: Observations of GW/TID oscillations in the F2 layer at low latitude during high and low solar activity, geomagnetic quiet and disturbed periods, J. Geophys. Res., 114, A02313, doi:10.1029/2008JA013448, 2009.

Lednyts'kyy, O., von Savigny, C., Eichmann, K.-U., Mlynczak, M. G.: Atomic oxygen retrievals in the MLT region from SCIAMACHY nightglow limb measurements, Atmos. Meas. Tech., 8, 1021-1041, doi: 10.5194/amt-8-1021-2015, 2015.

Limberger, M., Hernández-Pajares, M., Aragón-Ángel, A., Altadill, D., Dettering, D.: Long-term comparison of the ionospheric F2 layer electron density peak derived from ionosonde data and Formosat-3/COSMIC occultations, J. Space Weather Space Clim., 5, A21, 1-13, doi:10.1051/swsc/2015023, 2015.

Link, R., Cogger, L. L.: A reexamination of the O I 6300-Å nightglow, J. Geophys. Res., 93(A9), 9883-9892, doi:10.1029/JA093iA09p09883, 1988.

Lin, C. H., Liu, J. Y., Fang, T. W., Chang, P. Y., Tsai, H. F., Chen, C. H. and Hsiao, C. C.: Motions of the equatorial ionization anomaly crests imaged by FORMOSAT-3/COSMIC, Geophys. Res. Lett., 34, L19101, doi:10.1029/2007GL030741, 2007.

Lloyd, N., Manson, A. H., McEwen, D. J. and Meek, C. E.: A comparison of middle atmospheric dynamics at Saskatoon (52º N, 107º W) as measured by a medium-frequency radar and a Fabry-Perot interferometer, Journal of Geophysical Research, 95, 7653-7660, doi:10.1029/JD095iD06p07653.s, 1990.

López-González, M. J., Rodríguez, E., García-Comas, M., Costa, V., Shepherd, M. G., Shepherd, G. G., Aushev, V. M., and Sargoytchev, S.: Climatology of planetary wave type oscillations with periods of 2–20 days derived from O2 atmospheric and OH(6-2) airglow observations at mid-latitude with SATI, Ann. Geophys., 27, 3645-3662, doi:10.5194/angeo-27-3645-2009, 2009.

Luan, X., Wang, P., Dou, X., Liu, Y. C.-M.: Interhemispheric asymmetry of the equatorial ionization anomaly in solstices observed by COSMIC during 2007-2012, J. Geophys. Res., 120, 4, 3059-3073, doi:10.1002/2014JA020820, 2015.

Makela, J. J., Kelley, M. C., González, S. A., Aponte, N., McCoy, R. P.: Ionospheric topography maps using multiple-wavelength all-sky images, J. Geophys. Res., 106(A12), 29161–29174, doi:10.1029/2000JA000449, 2001.

Makela, J. J., Ledvina, B. M., Kelley, M. C., and Kintner, P. M.: Analysis of the seasonal variations of equatorial plasma bubble occurrence observed from Haleakala, Hawaii, Ann. Geophys., 22, 3109-3121, doi:10.5194/angeo-22-3109-2004, 2004

Mukherjee, G. K., Parihar, N., Niranjan, K. and Manju, G.: Signature of midnight temperature maximum (MTM) using OI 630 nm airglow, Indian Journal of Radio & Space Physics, 35, 14-21, 2006.

Nakamura, Y., Shiokawa, K., Otsuka, Y., Oyama, S., Nozawa, S., Komolmis, T., Komonjida, S., Neudegg, D., Yuile, C., Meriwether, J., Shinagawa, H., and Jin, H.: Measurement of thermospheric temperatures using OMTI Fabry–Perot interferometers with 70-mm etalon, Earth Planets and Space, 69, 1, 1-13, doi:10.1186/s40623-017-0643-1, 2017.

Parihar, N., Taori, A., Gurubaran, S., and Mukherjee, G. K.: Simultaneous measurement of OI 557.7 nm, O2 (0, 1) Atmospheric Band and OH (6, 2) Meinel Band nightglow at Kolhapur (17° N), India, Ann. Geophys., 31, 197-208, https://doi.org/10.5194/angeo-31-197-2013, 2013.

Parihar, N. and Taori, A.: An investigation of long-distance propagation of gravity waves under CAWSES India Phase II Programme, Ann. Geophys., 33, 547-560, doi:10.5194/angeo-33-547-2015, 2015.

Parihar, N., Singh, D. and Gurubaran, S.: A comparison of ground-based hydroxyl airglow temperatures with SABER/TIMED measurements over 23° N, India, Ann. Geophys., 35, 353-363, doi:10.5194/angeo-35-353-2017, 2017.

Paulino, I., Medeiros, A. F., Vadas, S. L., Wrasse, C. M., Takahashi, H., Buriti, R. A., Leite, D., Filgueira, S., Bageston, J. V., Sobral, J. H. A., and Gobbi, D.: Periodic waves in the lower thermosphere observed by OI630 nm airglow images, Ann. Geophys., 34, 293-301, doi:10.5194/angeo-34-293-2016, 2016.

Pavlov, A. V.: The role of the zonal E×B plasma drift in the low-latitude ionosphere at high solar activity near equinox from a new three-dimensional theoretical model, Ann. Geophys., 24, 10, 2553-2572, doi:10.5194/angeo-24-2553-2006, 2006.

Rao, C. S. R. and Malthotra, P. L.: A study of geomagnetic anomaly during I.G.Y., J. Atmos. Terr. Phys., 26, 11, 1075-1085, 1964.

Rama Rao, P. V. S., Srirama Rao, M., and Satyam, M.: Diurnal and seasonal trends in TEC values observed at Waltair, Indian Journal of Radio & Space Physics, 6 (3), 233-235, 1997.

Rao, H. N. R., and Sastri, J. H.: Characteristics of the equatorial midnight temperature maximum in the Indian sector, Ann. Geophys., 12, 2-3, 276-278, 1994.

Rastogi, R. G., and Klobuchar, J. A.: Ionospheric electron content within the equatorial F_2 layer anomaly belt, J. Geophys. Res., 95, 19045-19052, doi:10.1029/JA095iA11p19045, 1990.

Russell, J. P., Ward, W. E., Lowe, R. P., Roble, R. G., Shepherd, G. G., Solheim, B.: Atomic oxygen profiles (80 to 115 km) derived from wind imaging interferometer/upper atmospheric research satellite measurements of the hydroxyl and greenline airglow: local time – latitude dependence, J. Geophys. Res., 110, D15305, doi:10.1029/2004JD005570, 2005.

Sahai, Y., Bittencourt, J. A., Teixeira, N. R., Takahashi, H.: Simultaneous observations of OI 7774-Å and forbidden OI 6300-Å emissions and correlative study with ionospheric parameters, J. Geophys. Res., 86, 3657-3660, doi: 10.1029/JA086iA05p03657, 1981.

Scheer, J., Reisin, E. R.: Is there an influence of short-term solar activity variations on mesopause region airglow?, Adv. Space Res., 39, 8, 1248-1255, 2007.

Sethi, N. K., Dabas, R. S., and Vohra, V. K.: Diurnal and seasonal variations of hmF2 deduced from digital ionosonde over New Delhi and its comparison with IRI 2001, Ann. Geophys., 22, 453-458, doi:10.5194/angeo-22-453-2004, 2004.

Semenov, A. I.: Seasonal variations of hydroxyl rotational temperature, Geomagnetizm i Aeronomiia, 28, 333-334, 1988.

Shepherd, M. G.: WINDII observations of thermospheric O(1D) nightglow emission rates, temperature, and wind: 1. The northern hemisphere midnight temperature maximum and the wave 4, J. Geophys. Res., 121, 11,450–11,473, doi:10.1002/2016JA022703, 2016.

Shiokawa, K., Kadota, T., Otsuka, Y., Ogawa, T., Nakamura, T., Fukao, S.: A two-channel Fabry-Perot interferometer with thermoelectric-cooled CCD detectors for neutral wind measurement in the upper atmosphere, Earth Planets and Space, 55, 271-275, 2003.

Takahashi, H., Nakamura, T., Shiokawa, K., Tsuda, T., Lima, L. M., Gobbi, D.: Atmospheric density and pressure inferred from the meteor diffusion coefficient and airglow O_2b temperature in the MLT region, Earth Planets and Space, 56, 249-258, 2004.

Tinsley, B. A., Christensen, A. B., Bittencourt, J., Gouveia, H., Angreji, P. D., Takahashi, H.: Excitation of oxygen permitted line emissions in the tropical nightglow, J. Geophys. Res., 78, 7, 1174, doi:10.1029/JA078i007p01174, 1973.

Tinsley, B. A., Bittencourt, J. A.: Determination of F region height and peak electron density at night using airglow emissions from atomic oxygen, J. Geophys. Res., 80, 2333-2337, doi:10.1029/JA080i016p02333, 1975.

Vila, P., Rees, D., Merrien, P., and Kone, E.: Fabry-Perot interferometer measurements of neutral winds and F2 layer variations at the magnetic equator, Ann. Geophys., 16, 731-737, doi:10.1007/s00585-998-0731-4, 1998.

Yadav, S., Dabas, R. S., Das, Rupesh M., Upadhayaya, A. K., Sharma, K., Gwal, A. K.: Diurnal and seasonal variation of F2-layer ionospheric parameters at equatorial ionization anomaly crest region and their comparison with IRI-2001, Adv. Space Res., 45, 3, 361-367, doi:10.1016/j.asr.2009.08.018, 2010.

Yao, D. and Makela, J. J.: Analysis of equatorial plasma bubble zonal drift velocities in the Pacific sector by imaging techniques, Ann. Geophys., 25, 701-709, doi:10.5194/angeo-25-701-2007, 2007.

Zhao, B., Wan, W., Liu, L., and Ren, Z.: Characteristics of the ionospheric total electron content of the equatorial ionization anomaly in the Asian-Australian region during 1996–2004, Ann. Geophys., 27, 3861-3873, doi:10.5194/angeo-27-3861-2009, 2009.

Ann. Geophys. Discuss., https://doi.org/10.5194/angeo-2018-3
Manuscript under review for journal Ann. Geophys.
Discussion started: 11 January 2018

Figure Captions:

Figure 1. Coincidental COSMIC electron density profiles in the latitude-longitude grid of 5º x 5º centred on Allahabad (25.5º N, 81.9º E) on 14 October and 11 December 2009.

Figure 2. Nocturnal variation of the calibrated intensity of OI 777.4 nm and 630.0 nm emissions on 24 October 2009.

Figure 3. Frequency of occurrence of derived Nm over Allahabad during September – December 2009. Nm derived from OI 777.4 nm emission intensity using CP1 and CP2 calibration terms are shown in black and red bars, respectively.

Figure 4. Same as Figure 03 but for hmF2 derived from the ratio of $\sqrt{I_{7774}}$ and I_{6300}.

Figure 5. Nocturnal variation of Nm and hmF2 derived using *CP1 calibration term* on few nights October and December 2009.

Figure 6. Nocturnal variation of derived Nm and hmF2 on 14 October, 22 October (a slightly geomagnetic disturbed day), and 20 November 2009.

Figure 7. A limited comparison of airglow derived Nm with ionosonde measurements on 09 January 2016.

Figure 8. Sequence of Nm maps during 2000 – 2200 h IST on 09 January 2016 (Nm is expressed in cm^{-3}).

Figure 9. Same as **Figure** 6 but for hmF2 (hmF2 is expressed in km).

Ann. Geophys. Discuss., https://doi.org/10.5194/angeo-2018-3
Manuscript under review for journal Ann. Geophys.
Discussion started: 11 January 2018

Table Captions

Table No. 1. Calibration factor of OI 777.4 nm and 630.0 nm emission intensity inferred using the coincidental COSMIC profiles along with the azimuthal smearing of their tangent point trajectory.

Table No. 2. Comparison of the critical frequency of F2-layer (foF2) and corresponding peak of maximum electron density (hmF2) inferred from OI 777.4 nm and 630.0 nm emission intensity with the ionosonde measurements (foF2 and hpF2) on 16 September 2009.

Ann. Geophys. Discuss., https://doi.org/10.5194/angeo-2018-3
Manuscript under review for journal Ann. Geophys.
Discussion started: 11 January 2018

Annales Geophysicae Discussions

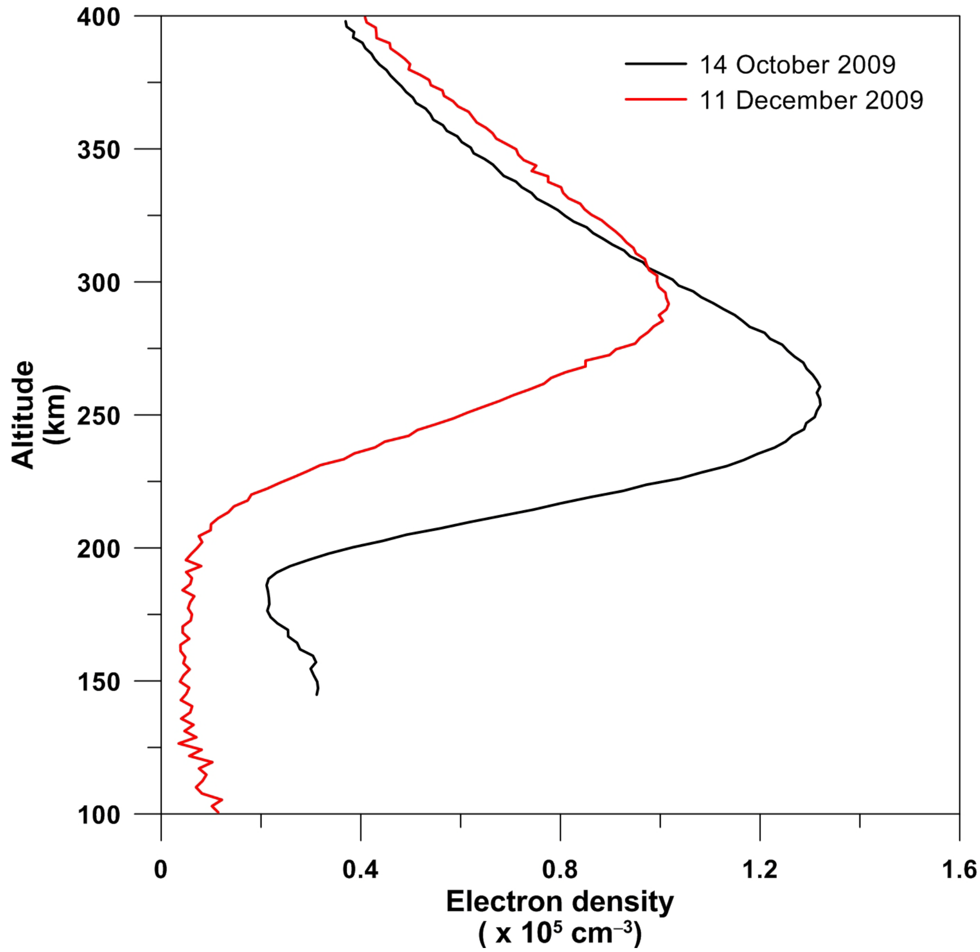

Figure 1. Coincidental COSMIC electron density profiles in the latitude-longitude grid of 5º x 5º centred on Allahabad (25.5º N, 81.9º E) on 14 October and 11 December 2009.

Ann. Geophys. Discuss., https://doi.org/10.5194/angeo-2018-3
Manuscript under review for journal Ann. Geophys.
Discussion started: 11 January 2018

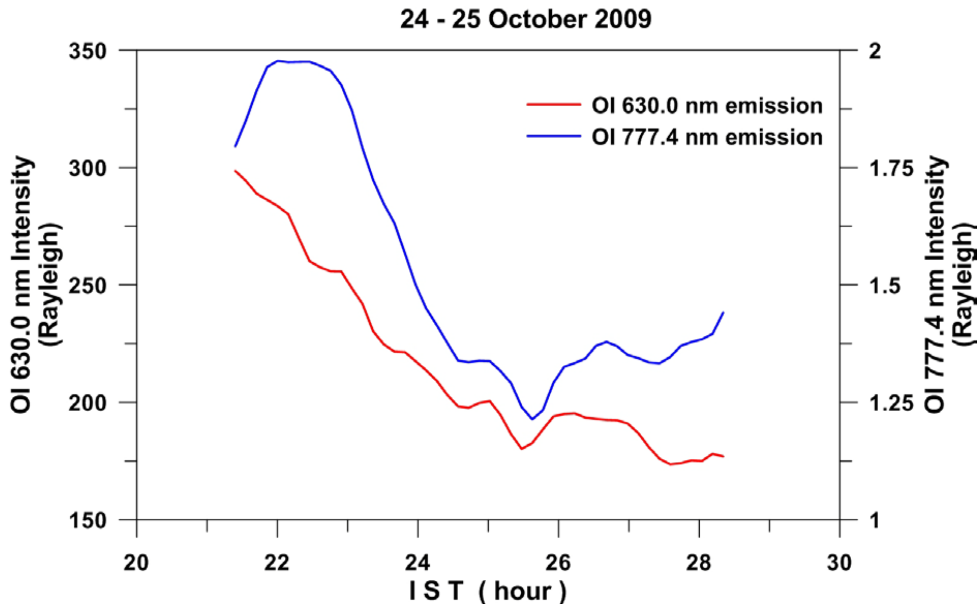

Figure 2. Nocturnal variation of the calibrated intensity of OI 777.4 nm and 630.0 nm emissions on 24 October 2009.

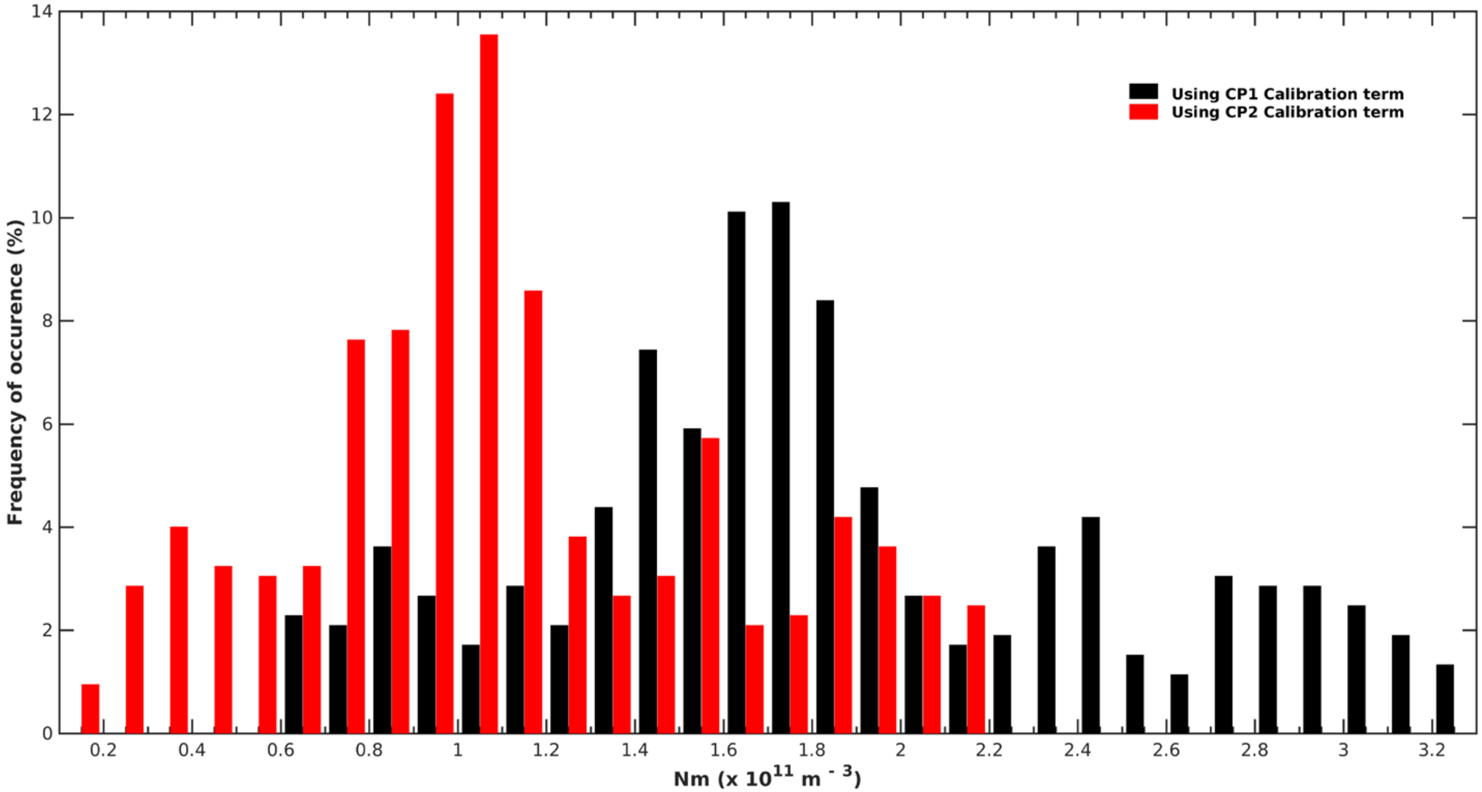

Figure 3. Frequency of occurrence of derived Nm over Allahabad during September – December 2009. Nm derived from OI 777.4 nm emission intensity using CP1 and CP2 calibration terms are shown in black and red bars, respectively.

Ann. Geophys. Discuss., https://doi.org/10.5194/angeo-2018-3
Manuscript under review for journal Ann. Geophys.
Discussion started: 11 January 2018

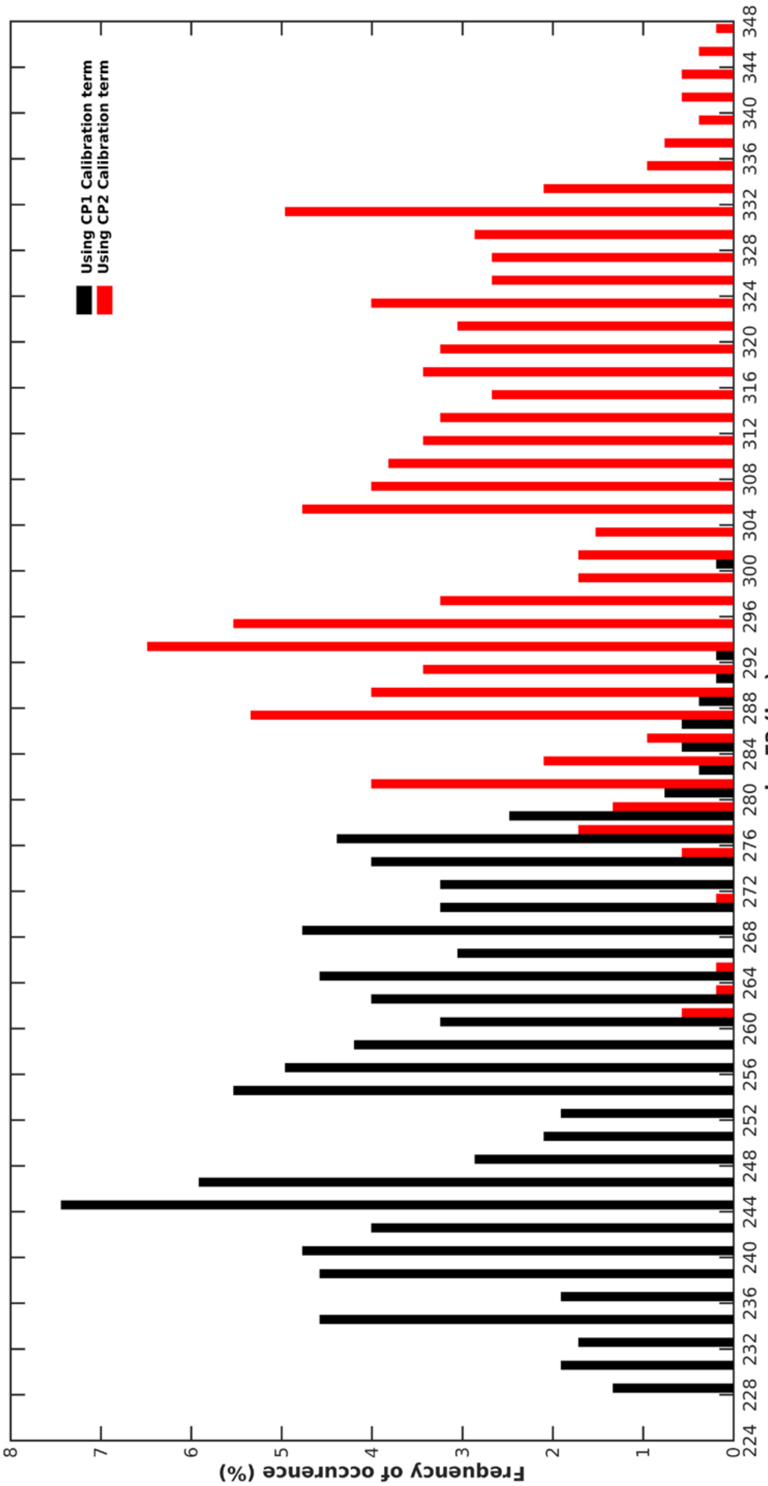

Figure 4. Same as Figure 03 but for hmF2 derived from the ratio of $\sqrt{I_{7774}}$ and I_{6300}.

Ann. Geophys. Discuss., https://doi.org/10.5194/angeo-2018-3
Manuscript under review for journal Ann. Geophys.
Discussion started: 11 January 2018

Annales Geophysicae Discussions

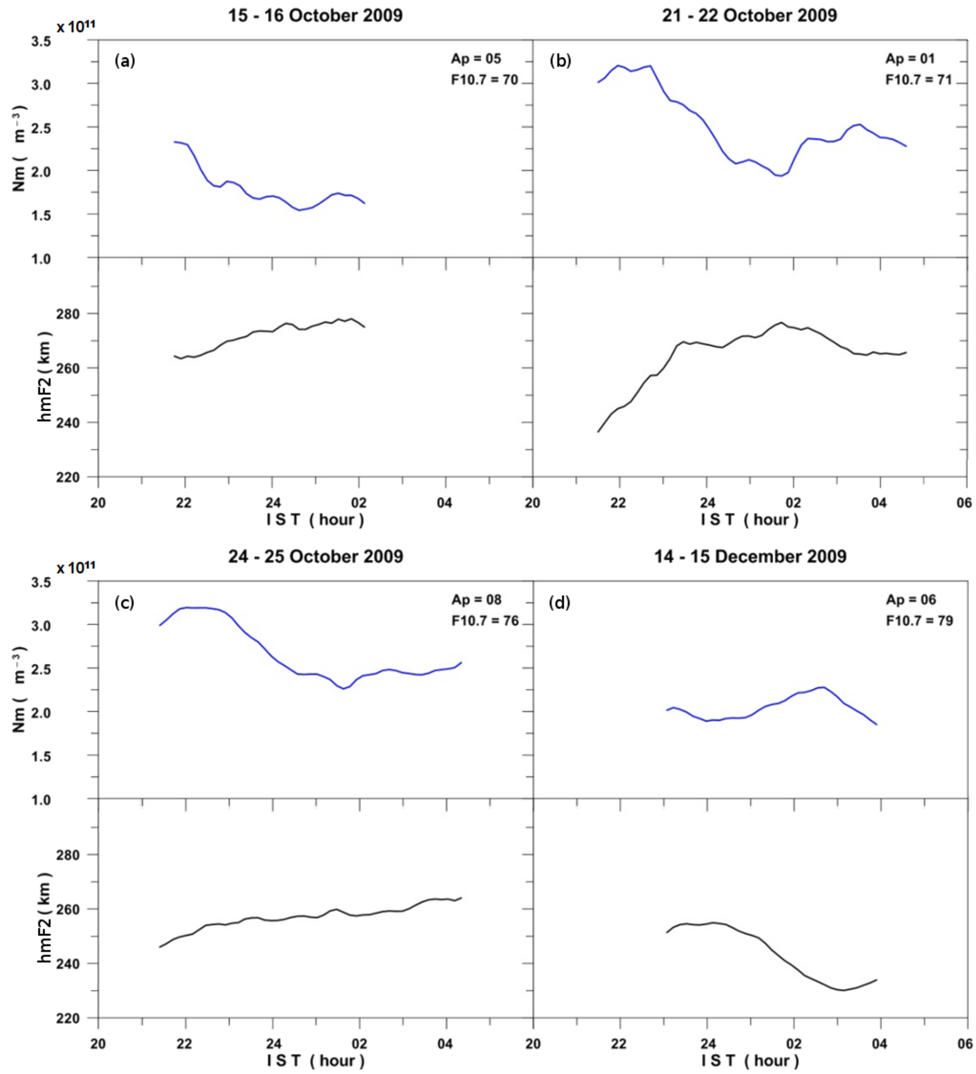

Figure 5. Nocturnal variation of Nm and hmF2 derived using *CP1 calibration term* on few nights October and December 2009.

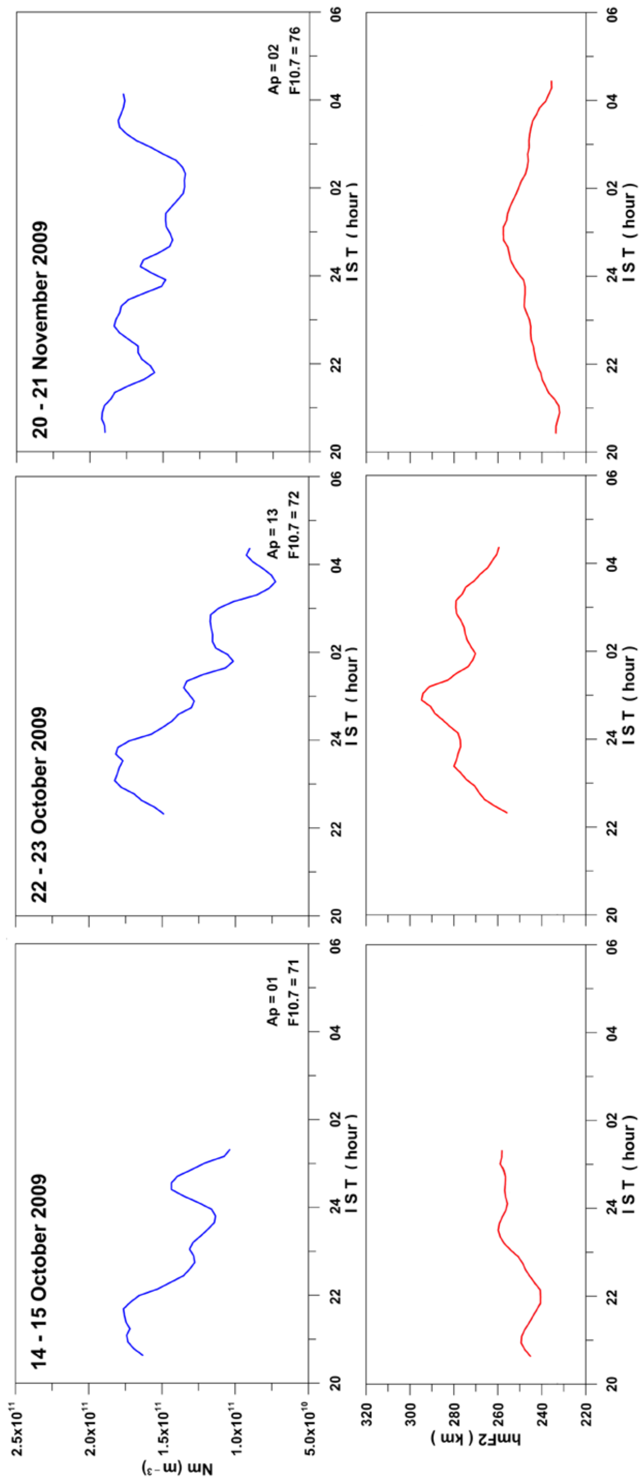

Figure 6. Nocturnal variation of derived Nm and hmF2 on 14 October, 22 October (a slightly geomagnetic disturbed day), and 20 November 2009.

Ann. Geophys. Discuss., https://doi.org/10.5194/angeo-2018-3
Manuscript under review for journal Ann. Geophys.
Discussion started: 11 January 2018

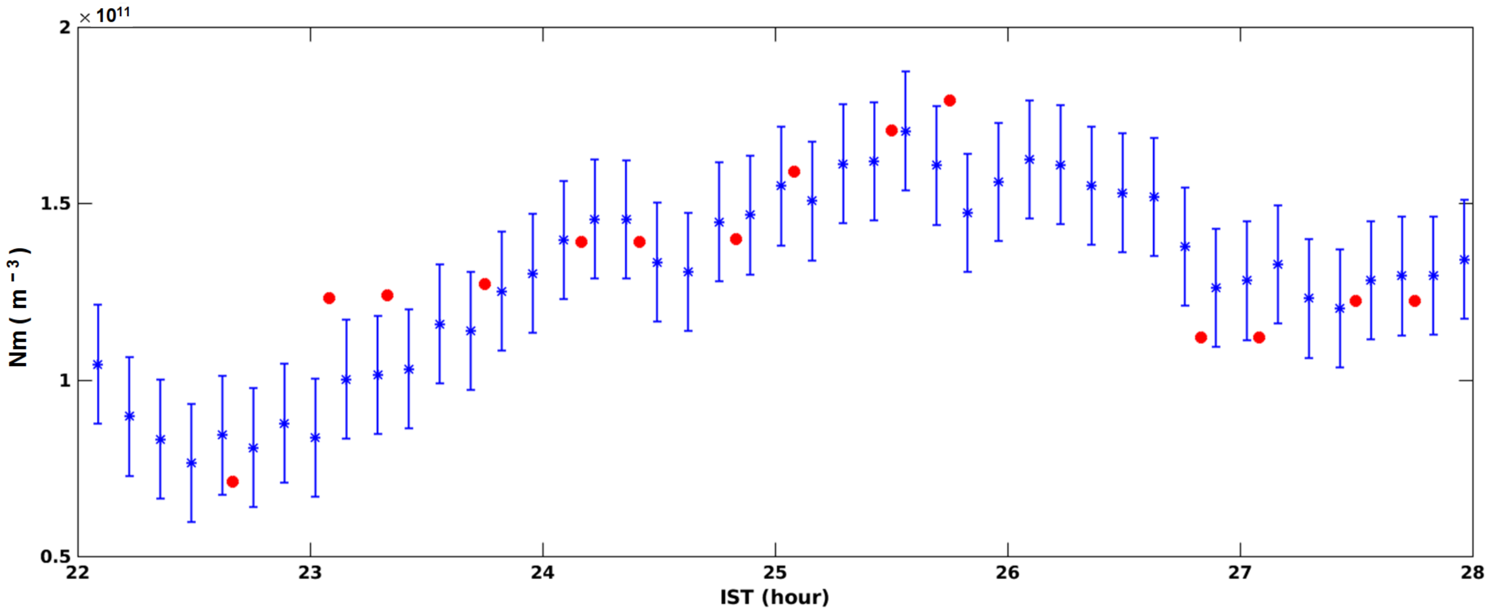

Figure 7. A limited comparison of airglow derived Nm with ionosonde measurements on 09 January 2016.

Ann. Geophys. Discuss., https://doi.org/10.5194/angeo-2018-3
Manuscript under review for journal Ann. Geophys.
Discussion started: 11 January 2018

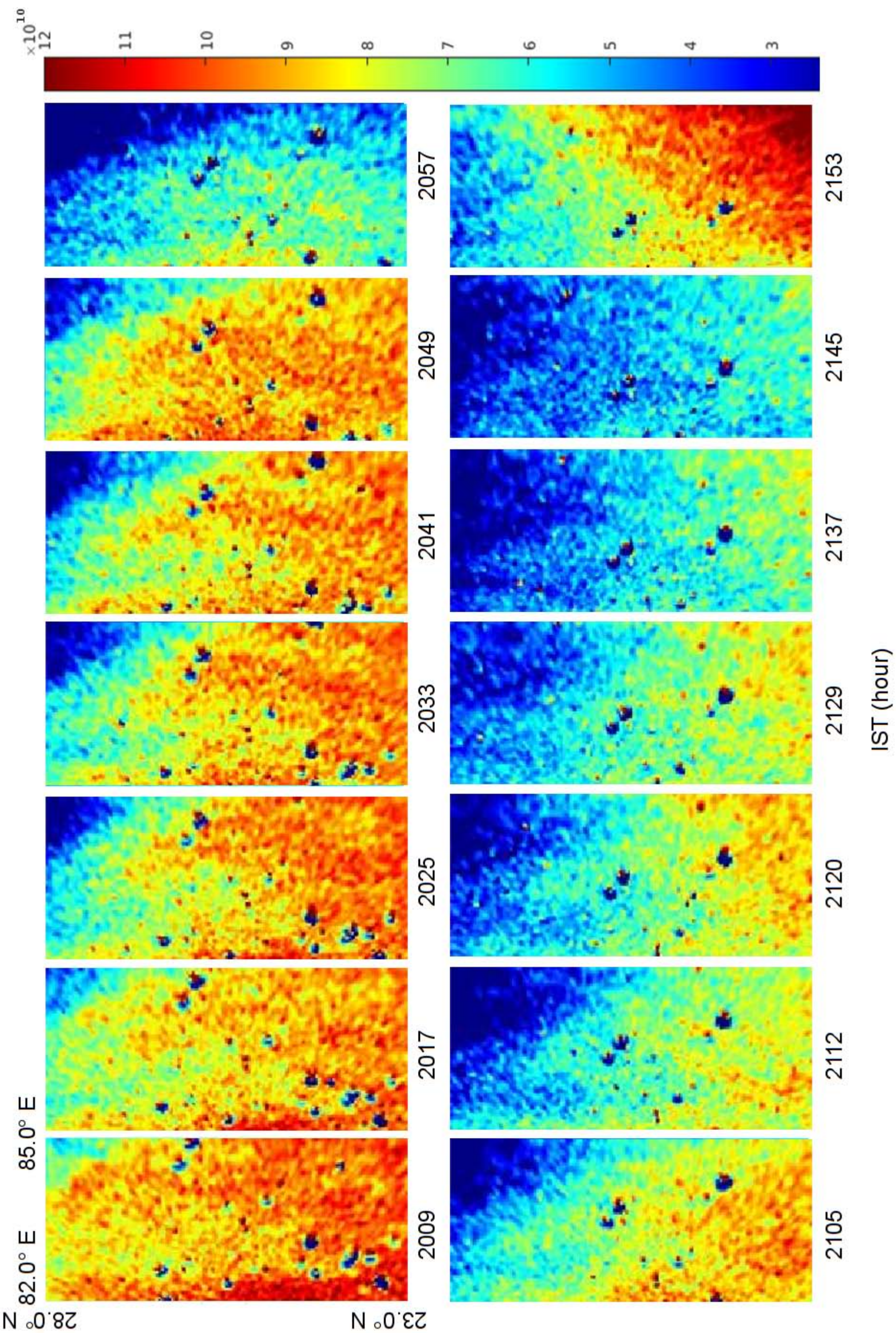

Figure 8. Sequence of Nm maps during 2000 – 2200 h IST on 09 January 2016 (Nm is expressed in cm^{-3}).

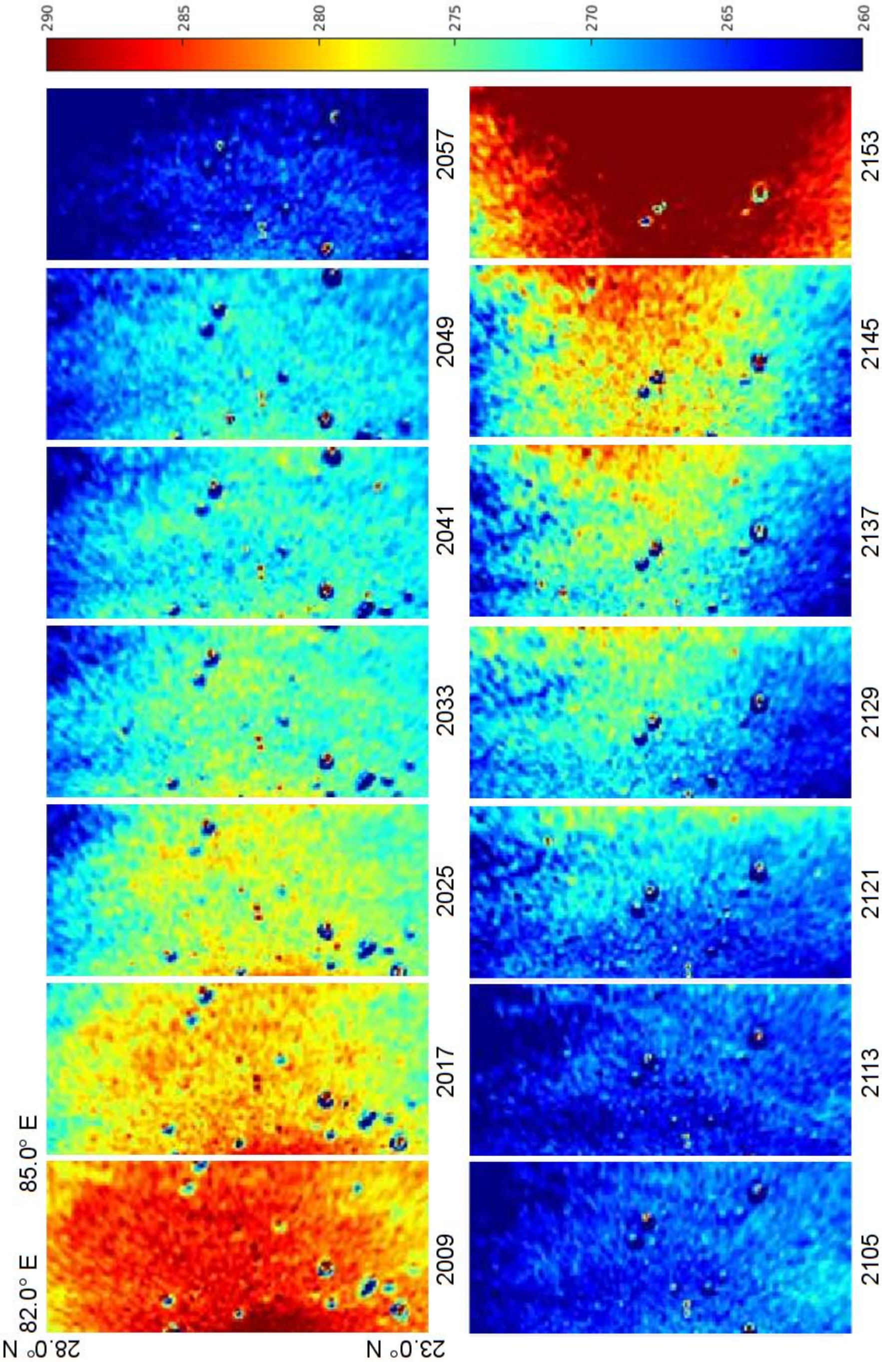

Figure 9. Same as **Figure** 6 but for hmF2 (hmF2 is expressed in km).

Ann. Geophys. Discuss., https://doi.org/10.5194/angeo-2018-3
Manuscript under review for journal Ann. Geophys.
Discussion started: 11 January 2018

Table No. 1. Calibration factor of OI 777.4 nm and 630.0 nm emission intensity inferred using the coincidental COSMIC profiles along with the azimuthal smearing of their tangent point trajectory.

Date	**Time (UT)**	**COSMIC electron density profile information**					**Inferred calibration factor for observed intensity**	
		Maximum of electron density (N_m) (in m^{-3})	Corresponding Altitude (hmF2) (in km)	Spatial spread of COSMIC Profile				
				Latitude (° N)	Longitude (° E)	Trajectory's Azimuth	OI 777.4 nm	OI 630.0 nm
14 October 2009	17.58	1.321 x 10^{11}	253.8	24.72 – 27.57	79.41 – 84.39	32.05 – 34.75°	5.4 x 10^{-3}	0.58
11 December 2009	18.40	1.017 x 10^{11}	291.8	25.05 – 26.38	79.42 – 84.37	00.08 – 02.37°	3.0 x 10^{-3}	0.15

Ann. Geophys. Discuss., https://doi.org/10.5194/angeo-2018-3
Manuscript under review for journal Ann. Geophys.
Discussion started: 11 January 2018

Table No. 2. Comparison of the critical frequency of F2-layer (foF2) and corresponding peak of maximum electron density (hmF2) inferred from OI 777.4 nm and 630.0 nm emission intensity with the ionosonde measurements (foF2 and hpF2) on 16 September 2009.

Airglow observations					Ionosonde measurements		
Time	Case I (CP1)		Case II (CP2)				
	foF2 (in MHz)	hmF2 (km)	foF2 (in MHz)	hmF2 (km)	Time	foF2 (in MHz)	hpF2 (km)
24.94	2.73	284.9	1.84	341.0	24.92	2.88	274.9
25.09	2.67	280.7	1.77	336.0	25.17	2.67	266.6
25.24	2.56	277.1	1.65	331.7	25.25	2.75	270.7
25.39	2.71	278.6	1.81	333. 5	25.33	2.66	270.7
25.54	2.73	276.9	1.84	331. 5	25.50	2.74	268.6
25.69	2.69	274.9	1.79	329.1	25.67	2.65	268.6